OPEN ACCESS
IOP Publishing | ISECAEP
Journal of Reliability Science and Engineering
J. Reliab. Sci. Eng. 1 (2025) 015005 (16pp)
https://doi.org/10.1088/3050-2454/adbaf8

Co-allocation of reliability-redundancy, spare parts and spacecraft trajectory for lunar habitation

Tongdan Jin* **and Ahsanul Abedin**

Ingram School of Engineering, Texas State University, San Marcos, TX 78666, United States of America

E-mail: tj17@txstate.edu

Received 24 December 2024, revised 23 February 2025
Accepted for publication 25 February 2025
Published 10 March 2025

Abstract

The complex and costly Earth–Moon logistics necessitates an innovative reliability paradigm to support the deployment and operations of lunar habitation base. To lay the groundwork for the new paradigm, this paper introduces a synergistic approach for optimizing reliability-redundancy, spares inventory, and spacecraft trajectory in the cislunar space. We propose a two-phase planning model to guide the establishment of a long-term human habitat on the Moon. Phase 1 allocates subsystem redundancy and base stock level to meet the reliability and availability goal at low mass cost. Phase 2 optimizes spacecraft fuel type, propellant mass and trajectory to minimize the total launch mass, including the habitat and spare parts of Phase 1. Notably, random spares demand, prolonged resupply, and limited transfer orbits are considered, making it first of its kind in co-optimizing redundancy, spares, rocket staging, and flight route. The redundancy-sparing-trajectory allocation model is demonstrated on the cislunar network with nine nodes and 23 velocity changes. Numerical study shows there exists a strong interdependence of launch mass, inventory lead time, transfer orbit, velocity change, and specific impulse. This study makes an early attempt to integrate space logistics theory into reliability and maintenance planning, potentially opening a new research direction for deploying reliable and cost-effective crewed bases in deep space.

Keywords: reliability-redundancy allocation, spare parts, space logistics, rocket staging, life support system

1. Introduction

Reliability and maintenance will be the critical considerations in future human flight missions to the Moon and Mars, because these deep-space explorations will operate in a logistically isolated environment for periods of months or even years. The major challenges in planning space logistics are the mass cost, flight time and distance, and environmental hazards. For instance, NASA's space shuttle costs about $1.5 billion to launch 27 tons of payload to Low Earth Orbit (LEO), or $54 500/kg. SpaceX's Falcon 9 currently advertises a cost of $2720/kg to launch 22.8 tons to LEO (Jones 2018), down by a factor of 20. However, the cost per unit mass is still too high to provide volume transportation and services to the public.

Prolonged time and distance constraints also complicate the design of spacecraft and resupply logistics for future manned deep space missions that will stretch from Earth to the Moon and Mars. Though the flight time from the Earth to the Moon takes only three days over a distance of 386 400 km, the

* Author to whom any correspondence should be addressed.

manufacturing of the spacecraft, including the rocket structure and propulsion system, usually takes months. Mars is, on average, 225 million km away from Earth, and at least six months of travel is required to reach the Red Planet. Autonomous space cargo vehicles, *in-situ* resource utilization (ISRU) extraction, and on-demand 3D printing are expected to address the distance and time challenges. More detailed discussions on the challenges of planning deep space logistics and supply chains can be referred to Baraniecka (2019) and the more recent one by Sawik (2023).

The space environment also presents tremendous hazards to interplanetary travel and permanent human habitation. These hazards include space radiation, debris from obsolete satellites, abandoned rocket stages, and mini-meteoroid strikes on the Moon or Mars surface. On-orbit resupply depots and lunar habitation (LH) bases will be exposed to such a harsh and unforgiving environment for years. The long endurance of these facilities requires careful deployment, operations and protection through reliability-redundancy (RR) design, predictive or data-driven maintenance, AI-based spare parts inventory management, and fully automated logistics solutions (Romero and Francisco 2020).

To address the costly and prolonged supply logistics issue in deep space, this paper proposes an integrated RR, spares inventory, and spacecraft trajectory optimization model to deploy manned facility on the Moon. The goal is to achieve high reliability and availability performance while minimizing the total launch mass including the physical habitat and spare parts. This integrated optimization problem is referred to as the redundancy-sparing-trajectory allocation (RSTA) model. To tackle the problem, a two-phase mixed integer programming model is formulated to investigate the vision of establishing a permanent habitat on Lunar South Pole (LSP) from system reliability, operational availability, and supportability perspective. In particular, Phase 1 aims to allocate redundant components and spares stock level to minimize the mass of the lunar habituation base with guaranteed reliability and availability. Based on the mass of the habitat and inventory of Phase 1, the aim of Phase 2 is to determine rocket stages, propellant type and mass, and trajectory from Earth to the Moon to minimize the total launch mass, including the payload.

Our contribution is to lay the groundwork for the joint planning of RR, spares logistics, rocket staging, and flight trajectory to facilitate deep space exploration. First, though RR, spare parts logistics and spacecraft trajectory have been studied intensively, we are not aware an integrated approach to redundancy, sparing and trajectory optimization has ever been reported in literature. Second, uncertain system failures and prolonged resupply lead times are explicitly taken into account, making the RSTA model a first of its kind to jointly optimize redundancy level, spares stocking, rocket staging, and vehicle routing. Third, the joint allocation model serves as a new concept in designing space vehicles as a growing number of nations are interested in returning to the Moon in the next 5–10 years (Nelson 2024). The proposed model is demonstrated on the cislunar logistics network comprised of nine nodes and up to 23 velocity changes.

The remainder of the article is organized as follows: section 2 reviews the related literature. Section 3 presents the reliability and availability model of the LH system, namely the life support and environmental control system. Section 4 introduces the Earth–Moon logistics network, including seven transfer nodes and the related velocity changes. In section 5 a two-phase optimization model is formulated to minimize the total launch mass. Section 6 performs numerical experiments and sensitivity analysis. Section 7 concludes the paper. Table 1 lists the notation and parameters of the RSTA model.

2. Literature review

2.1. RR allocation problem

Since the RSTA problem spans RR allocation, spare parts provisioning, and space supply chain logistics, the related works of these fields are reviewed respectively.

Reliability-redundancy allocation problem (RRAP) aims to find the optimal quantity of components (either active or standby) to maximize the system reliability and availability, or to minimize the cost subject to reliability criteria. Coit and Zio (2019) performed a comprehensive review of RRAP and chronologically divided this large body of literature into three periods: the rigid mathematical programming era, the pragmatism era, and the recently active reliability improvement era. The works and solution methods of the active reliability improvement era are discussed below as they are closely related to our paper. Ardakan *et al* (2016) advanced the RRAP field by implementing a mixed redundancy strategy, combining active and standby components, significantly improving system reliability over traditional strategies. Si *et al* (2019) combined Birnbaum importance measure with evolutionary algorithm to tackle RRAP. Ouyang *et al* (2019) introduced heterogeneous components into RRAP and proposed an improved particle swarm optimization (PSO) algorithm to solve it, emphasizing the noteworthy benefit of component heterogeneity to reliability growth. Zaretalab *et al* (2020) introduced multi-state components into the redundancy allocation problem, and a parameter-tuned memetic algorithm was used to optimize component source from multiple suppliers.

Recently RRAP is receiving much attention in reliability design of space systems. Wu and Wu (2017) proposed a hybrid heuristic measure to solve the RRAP of phased mission systems. They synthesize component importance measure with genetic algorithm (GA) to optimize new component reliability and redundancy of existing components. Li *et al* (2023) incorporated mixed redundancy strategy into crew survivability assessment of a multi-phase, manned spacecraft. The mission success probability in each phase is estimated by continuous-time Markov process coupled with binary decision diagram. An improved active-cold RRAP is solved using adaptive PSO algorithm. Chen *et al* (2024) considered the unique space environmental features, and devised a Bayesian importance measure to quantify subsystem's reliability contribution to the satellite communication system. A multi-objective RRAP is

Table 1. Model parameters and decision variables.

i, j	Index of nodes in the Earth–Moon logistics network
U	The number of subsystems of lunar habitat, for $u = 1, 2, \ldots, U$
V_u	The number of components or parts in subsystem u, for $v = 1, 2, \ldots, Vu$
$R_{\mathrm{LH}}(t)$	Reliability of lunar habitat at time t
A_{LH}	Availability of lunar habitat
$R^{\min}{}_{\mathrm{LH}}$	Reliability goal of lunar habitat at time t
$A^{\min}{}_{\mathrm{LH}}$	Availability goal for lunar habitat
D_{uv}	Demand for spare part (u, v)
$r_{uv}(t)$	Reliability of part (u, v) at time t
λ_{uv}	The failure rate of part (u, v) in lunar habitat
ΔV_{ij}	Velocity change from nodes i to j
I_{sp}	Specific impulse of propellant (unit: second)
J	The number of nodes in the cislunar network for i and $j = 1, 2, \ldots, J$
K	The number of rocket stages, for $k = 1, 2, \ldots, K$
N	The number of propellant types, for $n = 1, 2, \ldots, N$
m_{uv}	Unit mass of component or part (u, v)
m_{L}	Payload mass
m_{P}	Propellant or fuel mass of rocket or spacecraft
m_{E}	Empty mass of rocket or spacecraft
m_{S}	Structural mass of rocket or spacecraft
$m_{\mathrm{F},i}$	Full mass of the current rocket stage at node i
$m_{\mathrm{S},i}$	Structural mass of the current rocket stage at node i
$m_{\mathrm{P},i}$	Propellant mass of the current rocket stage at node i
ϕ_{ij}	Propellant consumption fraction from nodes i from j
g_0	Gravitational acceleration constant on Earth ($g_0 = 9.81$ m s^{-2})
τ	The mission duration
t_{HR}	Hands-on replacement time
t_{LT}	Spares inventory re-supply lead time
$t_{\mathrm{MDT},uv}$	Mean downtime of part (u, v) failure.
x_{ij}	Use of arc (i, j) by spacecraft, $x_{ij} = 1$ for use, otherwise 0, binary variable
y_u	Redundancy of subsystem u, for $u = 1, 2, \ldots, U$, integer decision variable
s_{uv}	Spare part inventory level for part (u, v), integer decision variable

formulated and solved to jointly optimize system reliability and cost using PSO.

2.2. Maintenance service logistics

Maintenance service logistics deals with the planning for parts replacement and provisioning. Wang and Syntetos (2011) developed a model for the joint optimization of spare parts inventory and maintenance inspection intervals using the delay-time concept. Wang (2012) further refined this approach by presenting a stochastic model for optimizing both spare parts inventory and preventive maintenance. Franciosi *et al* (2017) introduced sustainability metrics into periodic preventive maintenance models, highlighting significant cost savings and environmental benefits. Yan *et al* (2020) proposed a joint optimization model for maintenance and spare parts inventory in multi-unit systems, incorporating imperfect maintenance actions. Karabağ *et al* (2020) solved a similar problem using a partially observable Markov decision process where component failures are not fully visible. Zhu *et al* (2020) proposed using the system installed base and scheduled maintenance as advanced demand information to improve spare parts inventory control, revealing significant cost savings. Zheng *et al* (2021) developed a joint condition-based maintenance and spare parts provisioning policy for multi-unit systems with dual sourcing, focusing on the degradation levels of components. Recently, Zhu *et al* (2024) co-optimized maintenance time and spares inventory for onshore wind farms by considering dependencies between turbine usage and components' degradation. Zhang *et al* (2024) incorporating climate condition and seasonal variations into the predictive maintenance and replacement decision of wind turbine components,

2.3. Co-allocation of RR and spare parts

Efforts are also made to combine reliability data, redundancy strategy, and spare parts inventory to achieve the desired system reliability at a low cost. Jaarsveld and Dekker (2011) proposed a method to optimize spare parts stock levels using reliability-centered maintenance data, showing that costs can be reduced through redundancy information. Xie *et al* (2014) explicitly treated redundancy as a decision variable along with spares inventory to maximize the system's operational availability using a continuous-time Markov chain. Sleptchenko and van der Heijden (2016) further generalized this joint allocation approach by optimizing redundancy levels and spares inventories for k-out-of-N redundant systems with multiple part types. Olde Keizer *et al* (2017) introduced a model for the joint optimization of spares inventory management and condition-based maintenance, achieving just-in-time

failure replacement. Instead of assuming a static fleet size, Jin *et al* (2017) optimized component reliability, redundancy, and spares inventory for a variable system fleet through an adaptive (Q, r) policy to meet the non-stationary demand. Recently, Jin *et al* (2024) treated pro-active replacement time and repair capacity as endogenous variables along with redundancy and spares inventory in managing the fleet availability. Zhao *et al* (2018) showed that cold- and warm-standby redundancies and repair personnel together can achieve higher system availability, and that batch ordering is more cost-effective for slow-moving replenishment.

2.4. Space logistics and vehicle trajectory

An important branch of space logistics is to manage the flow of people and materials to and from space, as well as maintaining the operations of space infrastructure. Galluzzi *et al* (2006) emphasized the foundational importance of space supply chain management for manned missions, leading to Taylor *et al* (2007) developing a mathematical programming model to minimize transportation costs for interplanetary missions. Lin *et al* (2014) advanced this work by optimizing resupply logistics for the space station in LEO using GAs. Ho *et al* (2014) introduced a dynamic logistics network model for Mars exploration, incorporating ISRU, propellant production, and rocket staging. Ishimatsu *et al* (2016) further refined logistics strategies with a generalized multi-commodity network flow model, demonstrating significant mass reduction benefits for manned deep space exploration. Goodliff *et al* (2017) updated and expanded the logistics requirements for missions beyond LEO, focusing on consumables and packaging delivery. Lastly, Sawik (2023) integrated risk management and sustainability into space mission planning with a multi-objective optimization model. It concurrently minimizes risks and maximizes resource sustainability goals using a practical approach that assigns appropriate weights to each criterion and evaluates trade-offs to identify the best mission strategy.

The literature review shows the RRAP and maintenance service models address redundancy and spares provisioning, yet they are confined to the Earth environment. Space logistics, on the other hand, focuses on reducing the launch mass by optimizing rocket staging, propulsion technologies, and spacecraft trajectories, yet reliability and maintenance of space infrastructure during deployment are rarely considered. To fill this research gap, we propose a redundancy-sparing-trajectory optimization model for the deployment and sustainment of a long-term LH facility.

3. Reliability and availability of LHs

3.1. Environmental control and life support system (ECLSS)

A LH is expected to be a complex cyber-physical facility that plays an essential role in sustaining the daily living and operations of crew members. It is also referred to as the ECLSS by providing following functions: (a) supplying and recovering oxygen from carbon dioxide for crew breathing; (b) filtering particulates and microorganisms from the cabin air and maintaining cabin temperature, pressure, and humidity levels; (c) distributing cabin air between each room of the habitat; (d) purifying recycled water from multiple sources back to potable water; and (e) providing potable water for consumption, food preparation, and hygiene. Throughout the paper, ECLSS and LH are used interchangeably, representing a Moon-based life support facility where astronauts can live and work permanently.

ECLSS includes three major subsystems—Water Recovery (WR) subsystem, Air Revitalization (AR) Subsystem, and Oxygen Generation (OG) Subsystem. Figure 1 shows the hierarchical structure of the ECLSS at system, subsystem, module, and parts levels. Each subsystem is comprised of multiple modules, and each module again is decomposed into multiple components or parts.

Let $u = 1$, 2, and 3 be the index for WR, AR, and OG subsystems, respectively. To achieve high reliability and availability performance, parallel configurations are adopted by each subsystem. For example, the WR subsystem is configured with y_1 Water Recovery Module (WRM) in parallel. These WRM modules are identical units providing the same function. Similar interpretations can be applied to Air Revitalization Module (ARM) and Oxygen Generation Module (OGM). Hence the reliability block diagram of ECLSS can be modeled as a series–parallel system shown in figure 2.

Each module within a subsystem can be treated as a series configuration. For example, an WRM is comprised of V_1 components or parts connected in series where the subscript '1' represent the WR subsystem. Similar interpretation can be applied to ARM and OGM. Figure 3 shows the series configuration of WRM, ARM and OGM, respectively. Note that part (u, v) represents the component used in subsystem u for $u = 1$, 2, and 3 at location v for $v = 1, 2, \ldots, Vu$.

3.2. Reliability model of the ECLSS

The reliability block diagram of each module within a subsystem can be modeled as a series system shown in figure 3. For example, the function of WRM requires the simultaneous operations of part (1, 1), part (1, 2), and part (1, V_1) where V_1 is the total number of parts within the module. A similar interpretation can be applied to ARM and OGM, and the only difference is the number of the parts used. Let $u = 1$, 2, and 3 be the index for WR, AR, and OG subsystems, respectively. The reliability of the ECLSS can be expressed by

$$R_{\mathrm{LH}}(t) = \prod_{u=1}^{U}\left(1 - \left(1 - \prod_{v=1}^{V_u} r_{uv}(t)\right)^{y_u}\right) \qquad (1)$$

where y_u is the redundant level of subsystem u, and it is a decision variable. Note that U is the number of subsystems with $U = 3$ for the ECLSS in figure 2. If the lifetime of parts

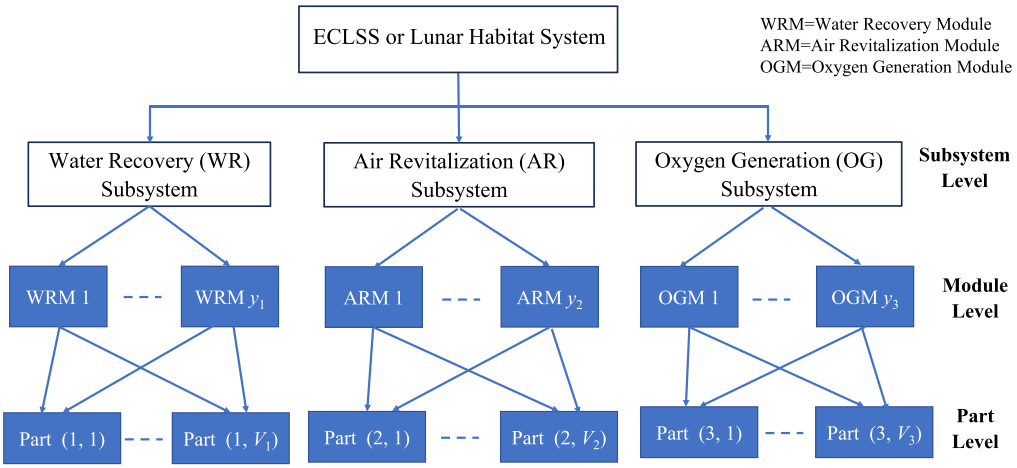

Figure 1. The hierarchical structure of ECLSS.

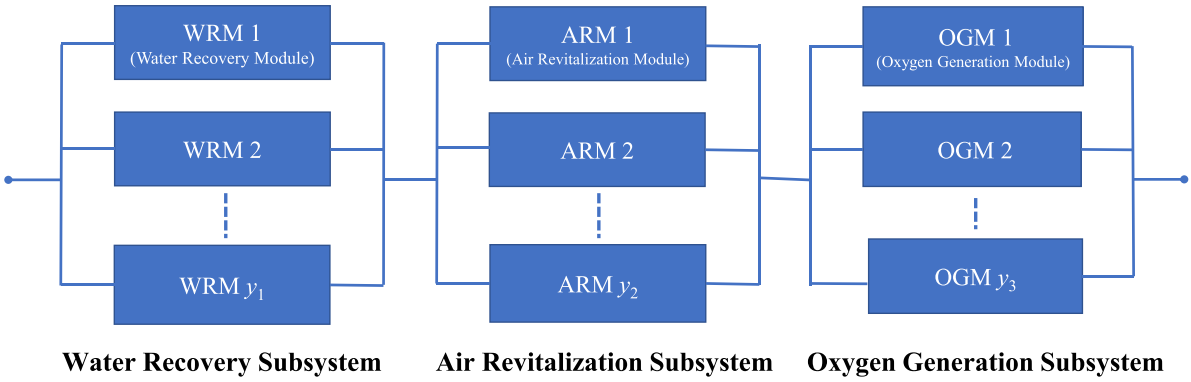

Figure 2. A series–parallel reliability model for ECLSS.

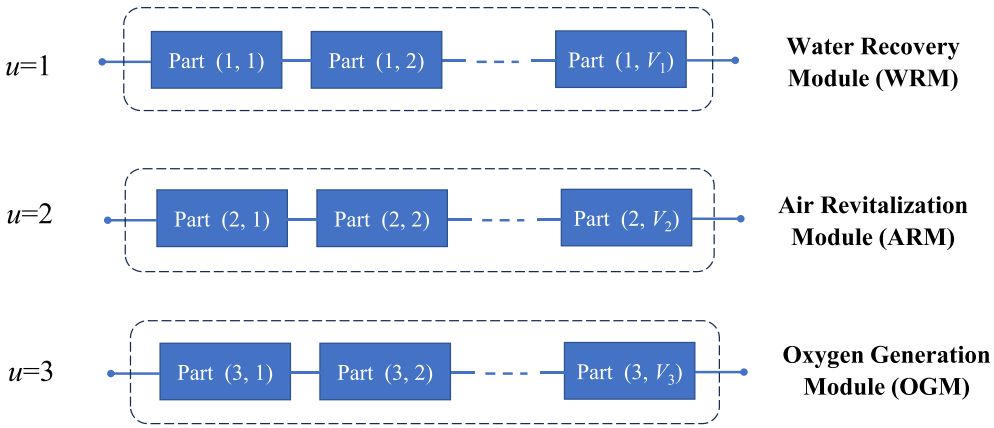

Figure 3. Series-system reliability configuration for WRM, ARM, and OGM.

within a subsystem is exponentially distributed with failure rate λ_{uv}, the reliability of the ECLSS can be expressed as follows

$$R_{\mathrm{LH}}(t) = \prod_{u=1}^{U}\left(1-\left(1-\prod_{v=1}^{V_u} \mathrm{e}^{-\lambda_{uv}t}\right)^{y_u}\right). \qquad (2)$$

3.3. Mean downtime (MDT) for replacement

To estimate the ECLSS availability, it is necessary to estimate the MDT due to repair and replacement activity. We consider two repair and replacement scenarios: (a) critical parts directly supplied from Earth; and (b) non-critical parts made by 3D printing on the Moon. Since the lead time of delivering a critical part from Earth takes much longer than the on-site printing

of non-critical parts, a critical parts inventory close to ECLSS is established to meet the maintenance demand.

A base inventory policy is adopted and also preferred if the demand for critical parts is intermittent coupled with prolonged lead time, which is the case for the ECLSS support. For a particular part type, a replenishment order is placed whenever the inventory level drops by one unit. Let s_{uv} be the base stock level of critical part (u, v). The MDT of a subsystem module (e.g. WRM, ARM and OGM) due to part (u, v) failure is estimated as follows:

$$t_{\mathrm{MDT},uv} = t_{\mathrm{HR}} + t_{\mathrm{LT}} \Pr\{D_{uv} > s_{uv}\}, \text{ for } u = 1,2,\ldots,U, \text{ and } v = 1,2,\ldots,V_u \tag{3}$$

where D_{uv} is a random variable representing the demand quantity for part (u, v) during inventory replenishment lead time. In addition, t_{HR} is the hands-on replacement time if an on-hand spare part is available. t_{LT} is the lead time for replenishing the spares inventory. For instance, the lead time for delivering a critical part from Earth to the Moon takes at least six days (Ishimatsu *et al* 2016). Equation (3) captures two replacement scenarios: if an on-hand spare item is available, the downtime is simply equal to t_{HR}. If the inventory is out of stock, $t_{\mathrm{LT}} \Pr\{D_{uv} > s_{uv}\}$ stands for the delay time awaiting the spare parts arrival from Earth. Equation (3) also shows MDT varies with part types because their lead-time demand and base stock level are different.

Similar to the assumption by Jiang *et al* (2011), Owens and de Weck (2018), and Jones (2019), the lifetime of part (u, v) is assumed to be exponential with failure rate λ_{uv}. Then the aggregate failures of y_u active units in ECLSS turn out to be a homogenous Poisson process with rate $y_u\lambda_{uv}$ (Detrell *et al* 2016). Now the stockout probability for part (u, v) can be estimated by,

$$\begin{aligned}\Pr\{D_{uv} > s_{uv}\} &= \sum_{h=s_{uv}+1}^{\infty} \frac{(y_u\lambda_{uv})^h \mathrm{e}^{-y_u\lambda_{uv}}}{h!} \\ &= 1 - \sum_{h=0}^{s_{uv}} \frac{(y_u\lambda_{uv})^h \mathrm{e}^{-y_u\lambda_{uv}}}{h!}.\end{aligned} \tag{4}$$

Note that s_{uv} is the base stock level of part (u, v). To meet the reliability criterion of the ECLSS, environmental screening tests are applied to components or modules prior to being transported to the Moon for installation. Therefore, infant mortality failures are largely eliminated from ECLSS. Since our study is focused on the initial installation and early operations of the ECLSS, a constant failure rate shall be appropriate because the system has not entered the degradation phase. Finally, substituting equation (4) into equation (3), the MDT of a module due to part (u, v) failure is obtained as

$$t_{\mathrm{MDT},uv} = t_{\mathrm{HR}} + t_{\mathrm{LT}} \left(1 - \sum_{h=0}^{s_{uv}} \frac{(y_u\lambda_{uv})^h \mathrm{e}^{-y_u\lambda_{uv}}}{h!}\right), \text{ for } u = 1,2,\ldots,U, \text{ and } v = 1,2,\ldots,V_u. \tag{5}$$

Equation (5) shows MDT highly depends on the spares stock level s_{uv} and the actual hands-on replacement time t_{HR}. Obviously, larger s_{uv} or shorter t_{HR} results in smaller MDT.

3.4. Operational availability of the ECLSS

The operational availability measures the percentage of the time that the ECLSS is functioning to provide potable water, oxygen, and other life-support necessities. Mathematically, the availability of single-item system, denoted as A_v, is defined as follows

$$A_v = \frac{\mathrm{MTBF}}{\mathrm{MTBF} + \mathrm{MDT}}, \tag{6}$$

where MTBF stands for meantime between failures. Since the ECLSS is a muti-item system, and its availability depends on the availability of individual subsystems, we first derive the operational availability of WR, AR, and OG subsystems based on the MTD of parts of each subsystem. By referring to the series configuration in figure 3, the module availability of subsystem u, denoted as $A_{m,u}$, is obtained by

$$A_{m,u} = \prod_{v=1}^{V_u} A_v = \prod_{v=1}^{V_u} \left(\frac{\frac{1}{\lambda_{uv}}}{\frac{1}{\lambda_{uv}} + t_{\mathrm{MDT},uv}}\right), \text{ for } u = 1,2,\ldots,U \tag{7}$$

where $1/\lambda_{uv}$ is the MTBF, and $t_{\mathrm{MDT},uv}$ is the MDT of part (u, v). Since components are connected in series, the module availability is the multiplication of the part availability. Each subsystem is comprised of y_u modules in parallel shown in figure 2, thus the subsystem availability is obtained as follows,

$$A_u = 1 - (1 - A_{m,u})^{y_u} = 1 - \left(1 - \prod_{v=1}^{V_u} \left(\frac{\frac{1}{\lambda_{uv}}}{\frac{1}{\lambda_{uv}} + t_{\mathrm{MDT},uv}}\right)\right)^{y_u}, \text{ for } u = 1,2,\ldots,U. \tag{8}$$

Since WR, AR and OG subsystems are connected in series, the availability of the ECLSS is the multiplication of individual subsystem availability. That is

$$A_{\mathrm{LH}} = \prod_{u=1}^{U} A_u = \prod_{u=1}^{U} \left(1 - \left(1 - \prod_{v=1}^{V_u} \left(\frac{\frac{1}{\lambda_{uv}}}{\frac{1}{\lambda_{uv}} + t_{\mathrm{MDT},uv}}\right)\right)^{y_u}\right). \tag{9}$$

By substituting equation (5) into equation (9), the availability of the ECLSS system can be expressed as a function of s_{uv} and y_u as follows

$$A_{\mathrm{LH}} = \prod_{u=1}^{U}\left(1-\left(1-\prod_{v=1}^{V_u}\left(\frac{\frac{1}{\lambda_{uv}}}{\frac{1}{\lambda_{uv}}+t_{\mathrm{HR}}+t_{\mathrm{LT}}\left(1-\sum_{h=0}^{s_{uv}}\frac{(y_u\lambda_{uv})^h \mathrm{e}^{-y_u\lambda_{uv}}}{h!}\right)}\right)\right)^{y_u}\right). \tag{10}$$

It is worth mentioning that A_{LH} plays a key role in the integrated redundancy-sparing-trajectory model, because it establishes an explicit connection with the spares inventory of different part types and the redundancy level of each subsystem.

4. Earth–Moon logistics network

4.1. Spacecraft trajectory and velocity change

The Earth–Moon logistics network, also called the cislunar supply chain, is shown in figure 4. The network starts from the Earth's surface and stretches to the Moon's surface via multiple intermediate or transfer nodes.

The cislunar logistics network in our study consists of nine nodes: EES, LEO, EML1, HLO, LLO, GEO, GTO, LES, and LSP. The full name and the role of these nodes are described in table 2. For example, EES stands for Earth Equatorial Surface and is the source node where spacecraft is launched to transport humans and materials to the Moon's ECLSS. Low Lunar Orbit (LLO) serves as a transfer node that relays the spacecraft further down to the Moon's surface. Unlike a stationary logistics node on Earth, a transfer node is indeed an orbit, circulating Earth or the Moon depending on its position. There are two destination nodes: Lunar Equatorial Surface (LES) and LSP where human habitats are to be established.

A velocity change is required to transfer a spacecraft from the current node (or orbit) to the new one. Let i be the current node and j be the new one, ΔV_{ij} stands for the velocity change or velocity difference between nodes i and j along the trajectory arc (i, j) shown in figure 4. The values of ΔV_{ij} for nine nodes are listed in table 3 (Taylor and de Weck 2005). For instance, when a spacecraft travels from LEO to HLO, the velocity change is $\Delta V_{26} = 3486$ m s^{-1}. For any arc between two nodes, ΔV_{ij} can be considered a constant or time-invariant value within the Earth–Moon cluster. Therefore, there is no need to consider a time-of-flight window in the cislunar logistics network.

4.2. Propellant and specific impulse in rocket staging

A variety of propellant systems are available including chemical, electric, and nuclear power. Chemical propulsion systems are broadly used in the commercial space industry. These include liquid oxygen and liquid hydrogen (LOX/LH2), liquid oxygen and kerosene (LOX/RP1), liquid oxygen and liquid methane (LOX/LCH4), and monomethyl hydrazine and nitrogen tetroxide (MMH/N2O4). Spacecraft using chemical propellants typically has two tanks, one for the oxidizing agent (e.g. O_2) and the other for the actual fuel (e.g. H_2). Multi-staging rockets are often used to transport materials on deep space missions. Figure 5 depicts a 3-stage spacecraft configuration enabling the achievement of three velocity changes through three burns.

The propellant is a critical asset in the space logistics system and must be accounted for as a design variable in our model. Propellant consumption primarily depends on three factors: (a) the velocity change in a trajectory arc; (b) the mass of the spacecraft including payload; and (c) the propellant type. In general, larger ΔV_{ij} or heavier spacecraft requires more propellant to reach the destination node.

The crucial difference between the various propellant types lies in their specific impulse value, denoted as I_{sp}. It measures how efficiently the spacecraft uses the propellant to generate thrust for velocity change ΔV_{ij}. Larger I_{sp} implies that less propellant is consumed for the spacecraft to gain the same velocity change. In the context of rocket propulsion, engines provide a constant thrust force; however, as fuel is consumed, the total mass of the spacecraft decreases, leading to an increasing acceleration. This non-linear velocity change is described by Tsiolkovsky's rocket equation as follows (Ho *et al* 2014, Ishimatsu *et al* 2016),

$$\Delta V_{ij} = I_{sp} g_0 \ln\left(\frac{m_i}{m_j}\right) \tag{11}$$

where g_0 is equal to 9.81 m s^{-2} on Earth, and m_i and m_j are the total mass of the spacecraft at the departure node i and arrival node j, respectively. This equation accounts for the exponential relationship between ΔV_{ij} and the fuel consumption from nodes i to j.

4.3. Propellant consumption

There are three different mass parameters relevant to the propellant consumption of spacecraft. These are propellant mass m_{P}, empty mass m_{E} and full mass m_{F}. In some literature, m_{E} and m_{F} are also called dry mass and wet mass, respectively. Their relationship is given as follows,

$$m_{\mathrm{F}} = m_{\mathrm{E}} + m_{\mathrm{P}}. \tag{12}$$

Furthermore, m_{E} is the sum of the spacecraft structure mass m_{S} and the payload mass m_{L}, that is

$$m_{\mathrm{E}} = m_{\mathrm{S}} + m_{\mathrm{L}}. \tag{13}$$

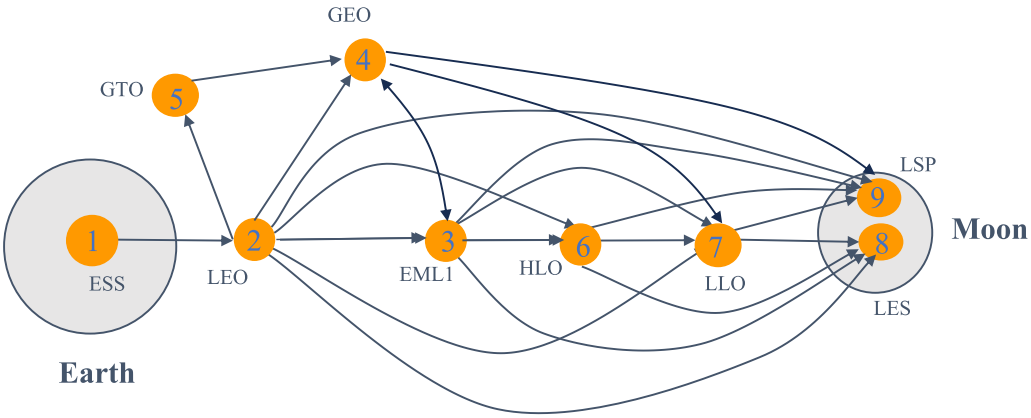

Figure 4. The Earth–Moon logistics network.

Table 2. Cislunar supply chain network nodes.

Node i	Abbreviation	Node name	Node function	Orbiting
1	EES	Earth's Equatorial Surface	Source	Stationary
2	LEO	Low Earth Orbit	Transfer	Earth
3	ELM1	First Earth–Moon Lagrange Point	Transfer	Earth
4	GEO	Geostationary Orbit	Transfer	Earth
5	GTO	Geostationary Transfer Orbit	Transfer	Earth
6	HLO	High Lunar Orbit	Transfer	Moon
7	LLO	Low Lunar Orbit	Transfer	Moon
8	LES	Lunar Equatorial Surface	Destination	Stationary
9	LSP	Lunar South Pole	Destination	Stationary

Table 3. $\triangle V_{ij}$ between orbits in the Earth–Moon network (unit: m s^{-1}).

Node	LEO ($j=2$)	EML1 ($j=3$)	GEO ($j=4$)	GTO ($j=5$)	HLO ($j=6$)	LLO ($j=7$)	LES ($j=8$)	LSP ($j=9$)
EES ($i=1$)	7900							
LEO ($i=2$)		3850	3900	2500	3486	4000	5865	5865
EML1 ($i=3$)			1380		366	880	2745	2745
GEO ($i=4$)		1380				2040	3940	3940
GTO ($i=5$)				1600				
HLO ($i=6$)						514	2379	2843
LLO ($i=7$)							1895	2098

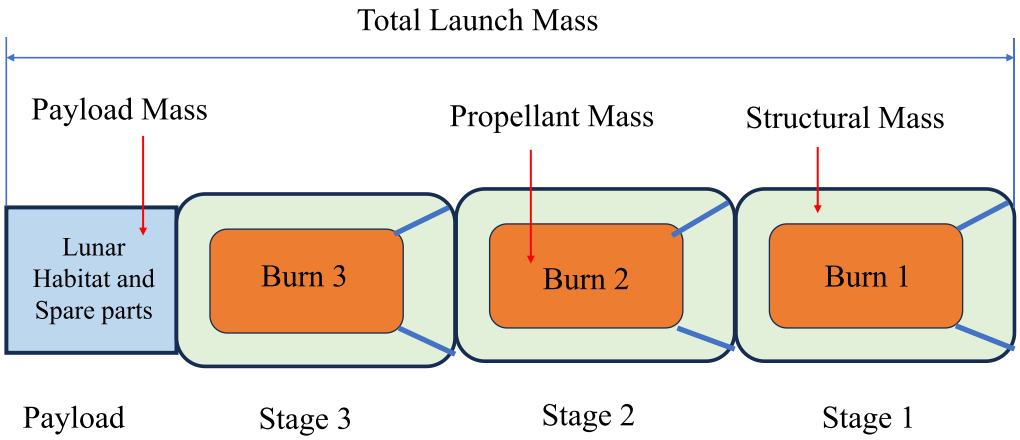

Figure 5. A spacecraft configuration with three propulsion stages.

The actual fuel use for a given arc (*i, j*) can be calculated based on m_{F}, m_{E}, and m_{L} along with I_{sp}. This requires the calculation of the propellant mass fraction, denoted as ϕ_{ij}, as follows

$$\phi_{ij} = 1 - \mathrm{e}^{-\frac{\Delta V_{ij}}{I_{sp} g_0}}. \tag{14}$$

The above result is directly derived from equation (11). Given the total mass at node *i*, equation (14) can estimate the amount of burned fuel over arc (*i, j*). The remaining fuel at node *j*, denoted as $m_{\mathrm{P},j}$ can be obtained as follows (Ishimatsu *et al* 2016, Blossey 2023)

$$m_{\mathrm{P},j} = (1 - \phi_{ij})\, m_{\mathrm{P},i} - \phi_{ij}\,(m_{\mathrm{S,i}} + m_{\mathrm{L}}) \tag{15}$$

or

$$m_{\mathrm{P},j} = m_{\mathrm{P},i} - \phi_{ij} m_{\mathrm{F},i} \tag{16}$$

where $m_{\mathrm{P},i}$ and $m_{\mathrm{P},j}$ are the propellant mass at nodes *i* and *j*, respectively. Also $m_{\mathrm{S},i}$ and $m_{\mathrm{F},i}$ are the structural mass and full mass at node *i*. Upon arrival at the destination node, no propellant is left or $m_{\mathrm{P},j} = 0$, therefore the propellant at its previous node *i* can be estimated through backward calculation. For a multi-stage rocket, when the current stage is burning, the total mass on top of the current stage is equivalent to the payload traveling from node *i* to node *j*. This is an important guideline to determine the necessary fuel for each stage in multi-stage rocket design. It is worth mentioning that the empty mass at the arrival node *j* may or may not change depending on the rocket staging design. If one stage has one burn only, the structural mass of the current stage will be jettisoned after the burn. Hence the structural mass departing from the current node to the next becomes smaller. However, if a stage accommodates multiple burns, the structural mass cannot drop off until after the last burn.

5. RSTA model

5.1. Model assumptions

The design, deployment, and sustainment of a lunar ECLSS can be formulated as a two-phase decision-making problem. In the first phase, we jointly allocate active redundant modules and spare parts to meet the reliability and availability criteria at low mass. In the second phase, we further minimize the total launch mass including ECLSS by determining rocket staging, propellant type and mass, and spacecraft trajectory. The following assumptions are made in the model formulation:

- Spacecraft is non-reusable and launched from EES.
- Spacecraft accommodates multiple stages with a single burn for each stage.
- Spacecraft enters LEO first and traverses a total of two transfer nodes prior to reaching the Moon.
- Components of ECLSS have an exponential lifetime with a constant failure rate.
- Modules of a subsystem are repairable on the Moon, but parts within a module are nonrepairable and must be resupplied from Earth.

5.2. Phase 1 for redundancy and spare parts allocation (RSPA)

The decisions of the Phase 1 model consist of two aspects: (1) allocating redundant modules within subsystem to meet the ECLSS reliability criterion, and (2) allocating spare parts inventory to lower the downtime of failure replacement, hence attaining system availability goal. The objective is to minimize the aggregate mass of ECLSS and spare parts, also known as payload. The RSPA problem is presented as follows:

Phase 1 Model: RSPA

Min:

$$f_1(\mathbf{s}, \mathbf{y}) = \sum_{u=1}^{U}\sum_{v=1}^{V_u} y_u m_{uv} + \sum_{u=1}^{U}\sum_{v=1}^{V_u} s_{uv} m_{uv}. \tag{17}$$

Subject to:

$$\prod_{u=1}^{U}\left(1 - \left(1 - \prod_{v=1}^{V_u} \mathrm{e}^{-\lambda_{uv}\tau}\right)^{y_u}\right) \geqslant R_{\mathrm{LH}}^{\min} \tag{18}$$

$$\prod_{u=1}^{U}\left(1 - \left(1 - \prod_{v=1}^{V_u}\left(\frac{\frac{1}{\lambda_{uv}}}{\frac{1}{\lambda_{uv}} + t_{\mathrm{HR}} + t_{\mathrm{LT}}\left(1 - \sum_{h=0}^{s_{uv}} \frac{(y_u\lambda_{uv})^h \mathrm{e}^{-y_u\lambda_{uv}}}{h!}\right)}\right)\right)^{y_u}\right) \geqslant A_{\mathrm{LH}}^{\min} \tag{19}$$

$$y_u \in \{1,\ 2,\ 3\ldots\}, \quad \text{for}\, u = 1,\ 2,\ \ldots, U. \tag{20}$$

$$s_{uv} \in \{0,\ 1,\ 2,\ 3\ldots\}, \quad \text{for}\, u = 1, 2, \ldots, U, \text{ and}\, v = 1, 2, \ldots, V_u. \tag{21}$$

In the objective function (17), the first term sums the masses of WR, AR, and OG subsystems. The second term is the spare parts mass of the components for three subsystems. $\boldsymbol{s} = [s_{11},\ s_{12},\ \ldots,\ s_{U,1},\ \ldots,\ s_{U,Vu}]$ are the decision variables for the base stock level of part (*u, v*). Also $\mathbf{y} = [y_1,\ y_2,\ \ldots,\ y_U]$ are the decision variables for subsystem redundancy level. Constraint (18) defines the reliability criterion of the ECLSS during mission endurance τ, and $R_{\mathrm{LH}}^{\min}$ is the required reliability level. Constraint (19) defines the availability criterion of the ECLSS system, and $A_{\mathrm{LH}}^{\min}$ is the required level. Constraints (20) to (21) simply state the non-negativity of the integer decision variables.

5.3. Phase 2 for rocket staging and trajectory planning

In Phase 2, our objective is to determine the propellant type, fuel mass in each stage, and the spacecraft trajectory to transport ECLSS and spare parts from Earth to the Moon surface. The Phase 2 model is called the Spacecraft Staging and Trajectory Planning (SSTP) problem, which is formulated as follows,

Phase 2 Model: SSTP
Min:

$$f_2(\mathbf{x};\mathbf{s},\mathbf{y}) = \sum_{k=1}^{K}\sum_{n=1}^{N}(m_{S,kn}+m_{P,kn}) + f_1(\mathbf{s},\mathbf{y}). \quad (22)$$

Subject to:

$$\sum_{j=2}^{J} x_{1j} = 1, \qquad \text{for } i = 1. \quad (23)$$

$$\sum_{i=1}^{J-1} x_{iJ} = 1, \qquad \text{for } j = J. \quad (24)$$

$$\sum_{i\neq j}^{J-1} x_{ij} = \sum_{l\neq j}^{J-1} x_{jl} \qquad \text{for } j = 2,\ 3,\ \ldots, J-1 \quad (25)$$

$$\sum_{i=1}^{J-1}\sum_{j=2}^{J} x_{ij} \leqslant K \quad (26)$$

$$x_{12} = 1 \quad (27)$$

$$\sum_{i=1}^{j-1}\sum_{l=i+1}^{j} x_{il} = z, \qquad \text{for } j = 2,\ 3,\ \ldots, J. \quad (28)$$

$$\phi_{ij}x_{ij}\left[f_1(\mathbf{s},\mathbf{y}) + \sum_{k=z}^{K}\sum_{n=1}^{N}(m_{S,kn}+m_{P,kn})\right] = m_{P,zn}\ ,\ \forall i \text{ and } j. \quad (29)$$

$$m_{S,kn} = \alpha_{kn}m_{P,kn}, \ \text{ for } k = 1,\ 2,\ \ldots, K, \text{ and } n = 1,\ 2,\ \ldots, N. \quad (30)$$

$$x_{ij}\{0,1\}, \text{ for } i \neq j. \quad (31)$$

In objective function (22), the first term represents the initial mass of the spacecraft comprised of the structural and fuel masses of all K stages. Particularly, $m_{P,kn}$ is the propellant mass of fuel type n in Stage k. Also $m_{S,kn}$ is the structural mass of Stage k if using fuel type n. The second term is the payload or the mass of ECLSS and spare parts obtained from Phase 1 model. The mass in equation (22) is also called the total launch mass. $\mathbf{x} = [x_{12}, x_{13}, \ldots., x_{N-1,N}]$ are the binary decision variables, representing the arc through which the spacecraft travels. If $x_{ij} = 1$, the spacecraft travels from nodes i to j, otherwise $x_{ij} = 0$. Also, J is the destination node LSP with $J = 9$, and the launch node is EES with $i = 1$.

Constraint (23) ensures that the spacecraft must depart from EES. Constraint (24) ensures that the spacecraft must arrive at LSP ($j = J$). Constraint (25) ensures that the spacecraft arrives at node j, it must leave node j expect for the destination node. Constraint (26) states that at most K arcs are traveled by the spacecraft between EES and LSP. If a rocket has three stages with one burn for each stage, it implies $K = 3$. Constraint (27) prescribes a common practice in space missions in which a spacecraft launched from the EES must enter the LEO first. Constraint (28) states that the number of arcs traveled equals the number of stages burned. Constraint (29) computes the propellant use of rocket stage when transferring from nodes i to j where ϕ_{ij} is dependent on fuel type n. Constraint (30) defines the structural ratio by propellant type in each stage. Constraint (31) states the nature of the binary decision variables.

5.4. Solution algorithm

The Phase 1 model belongs to the mixed integer non-linear programming (MINLP) problem. Since it involves the complexity of nonlinearity and the combinatorial nature with potential non-convexity, there is no effective method to solve this type of problem. Metaheuristic algorithms such as GA are often used to solve MINLP problems like RR allocation (Kim and Kim 2017, Peiravi *et al* 2022). The pseudocode of GA for Model RSPA is elaborated below

$N_{gn}{}^{max}$ = the maximum number of generations
N_{pop} = the number of chromosomes in population
P_c = the probability of the crossover operation
P_m = the probability of the mutation operation
Pop(g) = the gth generation for $g = 1, 2, \ldots, N_{gn}{}^{max}$
Ch = [y_1, y_2, …, y_U, s_{11}, s_{12}, …, $s_{U,1}$, …, $s_{U,Vu}$], representing a chromosome, and the number of genes equals $U + V_1 + \ldots + Vu$.

The program starts from here:
While $g < N_{gn}{}^{max}$, do

- Generating random value of Rnd_c, Rnd_1, and Rnd_2 between $U[0, 1]$,
- Ch_1, Ch_2 = choose two chromosomes from Pop(g),
- Remove Ch_1 and Ch_2 from Pop(g),

If $Rnd_c < P_c$, then
  Crossover Ch_1 and Ch_2 to create two new offsprings Ch_3 and Ch_4,
else
  $Ch_3 = Ch_1$, and $Ch_4 = Ch_2$,
endif
if $Rnd_1 < P_m$, then
  Performing the mutation on Ch_3,
endif
if $Rnd_2 < P_m$, then
  Performing the mutation on Ch_4,
end if

- Using objective function $f_1(\mathbf{s}, \mathbf{y})$ in Model RSPA to test Ch_1, Ch_2, Ch_3 and Ch_4, select two fittest chromosomes and add them to next generation of population Pop($g + 1$),
- $g = g + 1$,
- Repeating crossover, mutation, and fitness test for all N_{pop} chromosomes.

End while

Since Phase 2 Model SSTP involves four types of propellants and nine nodes with 21 arcs or links. We decided to solve SSTP using Dijkstra's algorithm because this algorithm can effectively find the minimum launch mass in a weighted graph. The details of algorithm can be referred to Fink *et al* (2019).

The cislunar network in figure 4 can be treated as a weighted graph. The weight of individual links is governed by the propellant mass fraction in equation (14). A link with larger ΔV_{ij} requires higher consumption of fuel given the same payload. On the other hand, larger I_{sp} implies less fuel use. Hence ΔV_{ij} and I_{sp} jointly determine the weight of the link between nodes i and j. Using Dijkstra's algorithm, the route from EES to LSP that results in the lowest launch mass is the optimal trajectory. Both the metaheuristics and Dijkstra's algorithms are coded in MATLAB and executed in a PC with an Intel (R) Core (TM) i5-7200U CPU @ 2.5 GHz, 4 Core(s), 24 GB memory, and 4 Logical Processors.

6. Numerical experiment

6.1. Model input data

The ECLSS in figure 2 is used to demonstrate the application of the proposed two-phase allocation model. Since the lunar ECLSS is still in its infant research and development stage, actual reliability and mass data of individual components and the whole system are not available to the public. Based on the study of West *et al* (2016), a generic ECLSS system is used to demonstrate the application of the proposed model. Table 4 lists the failure rate and mass of individual parts used in WRM, ARM, and OGM, respectively. Component failure rates are estimated based on the ECLSS of low orbit space stations (Owens and de Weck 2018, Jones 2019). The WRM comprises three parts in series, the ARM comprises five parts in series, and the OGM comprises four parts in series.

For this analysis, we consider a three-stage, three-burn spacecraft system shown in figure 5, and calculate the initial structural and propellant masses of each stage. For Stage k, the structural mass is related to the propellant mass through structural ratio α_{kn} as follows,

$$\alpha_{kn} = \frac{m_{\mathrm{S},kn}}{m_{\mathrm{P,kn}}}, \text{for} k = 1, 2, \ldots, K, \text{ and} n = 1, 2, \ldots, N \quad (32)$$

where $m_{\mathrm{S},kn}$ is the structural mass of Stage k if using fuel type n, and $m_{\mathrm{P},kn}$ is the fuel mass of type n in Stage k. Four types of chemical fuels can be chosen for rocket staging: LOX-LH2, LOX-RP1, MMH-N2O4, and LOX-LCH4. Table 5 lists the corresponding values of I_{sp} and α given by Klem (2017).

6.2. Results and discussion of Phase 1 model

In Phase 1, Model RSPA is solved using both GA and iterative method (IM) based on the WRM, ARM and OGM data of table 4. Other necessary input data include τ, t_{HR}, t_{LT}, $R_{\mathrm{LH}}{}^{\mathrm{min}}$ and $A_{\mathrm{LH}}{}^{\mathrm{min}}$. IM is able to find the global optimality by searching the entire solution space, and the results are used to compare with the GA.

Table 6 summarizes the results of six cases solved by GA and IM, respectively. Case 1 serves as the baseline study with $\tau = 1$ year, $t_{\mathrm{HR}} = 24$ h, $t_{\mathrm{LT}} = 183$ d, $R_{\mathrm{LH}}{}^{\mathrm{min}} = 0.95$, and

Table 4. Component reliability and mass of module WRM, ARM and OGM.

Index (u)	Module	Part (u, v)	λ_{uv} (failure/year)	m_{uv} (kg)	Unit cost ($)
1	WRM	(1, 1)	0.11	80	62 837
		(1, 2)	0.10	100	63 055
		(1, 3)	0.09	120	51 342
2	ARM	(2, 1)	0.22	180	127 343
		(2, 2)	0.21	190	78 576
		(2, 3)	0.20	200	117 811
		(2, 4)	0.19	210	91 968
		(2, 5)	0.18	220	71 729
3	OGM	(3, 1)	0.16	120	98 150
		(3, 2)	0.15	130	85 143
		(3, 3)	0.14	150	158 453
		(3, 4)	0.13	170	163 185

Table 5. Specific impulse and structural mass ratio of propellants.

Type	Propellant	I_{sp} (s)	α for Stage 1 ($k = 1$)	α for Stage 2 ($k = 2$)	α for Stage 3 ($k = 3$)
$n = 1$	LOX-LH2	450	0.09	0.14	0.14
$n = 2$	LOX-RP1	290	0.068	0.08	0.08
$n = 3$	MMH-N2O4	330	0.11	0.13	0.13
$n = 4$	LOX-LCH4	355	0.085	0.10	0.10

$A_{\mathrm{LH}}{}^{\mathrm{min}} = 0.9999$. A similar availability criterion is used by Detrell *et al* (2016) to design Mars' ECLSS. The reliability goal of 0.95 is defined at $\tau = 1$ year on the premise that no replacement is performed if components fail, representing the worst scenario with no spares inventory. For Case 1, GA requires a total mass of 12 410 kg, including 11 920 kg for ECLSS and 490 kg for spares. The achieved reliability is $R_{\mathrm{LH}} = 0.952$, and the achieved system availability $A_{\mathrm{LH}} = 0.99991$. IM results in a slightly better solution than GA by reducing the spares mass by 120 kg, or 1% lower than GA. Table 7 shows the redundancy allocation and base stock level for Case 1 obtained by GA and IM. Both algorithms result in the same redundancy allocation $\mathbf{y} = [5, 7, 6]$, but GA requires three spares $[s_{21} = 1, s_{22} = 1, s_{31} = 1]$ and IM does not need s_{31}.

Case 2 examines how $R_{\mathrm{LH}}{}^{\mathrm{min}}$ influences redundancy and spares allocation. We reduce $R_{\mathrm{LH}}{}^{\mathrm{min}}$ from 0.95 to 0.9 at $\tau = 1$ year. The solution opts to reduce the redundancy for each subsystem down from $\mathbf{y} = [5, 7, 6]$ to [3, 6, 5] shown in table 7. Use GA as example, it is observed that the total number of spare parts increases from 3 to 6, but the total mass drops from 12 410 kg to 10 710 kg, or down by 13.7% as opposed to Case 1.

Cases 3 investigates how the mission endurance τ influences redundancy and spares decision. We let τ reduce from

Table 6. Mass comparison between GA and iterative algorithms for Phase 1.

Case	τ (yr)	t_{HR} (hr)	t_{LT} (day)	R_{LH}^{min}	A_{LH}^{min}	R_{LH}	A_{LH}	ECLSS Mass (kg)	Spares Mass (kg)	Total Mass (kg)	Mass Increase (%)
1 (IM)	1	24	183	0.95	0.9999	0.952	0.999 91	11 920	370	12 290	
1 (GA)	1	24	183	0.95	0.9999	0.952	0.999 91	11 920	490	12 410	1.0%
2 (IM)	1	24	183	0.90	0.9999	0.905	0.999 91	9750	960	10 710	
2 (GA)	1	24	183	0.90	0.9999	0.905	0.999 91	9750	960	10 710	0.0%
3 (IM)	0.5	24	183	0.95	0.9999	0.958	0.999 92	6610	1750	8360	
3 (GA)	0.5	24	183	0.95	0.9999	0.958	0.999 91	6610	1830	8440	1.0%
4 (IM)	1	48	183	0.95	0.9999	0.952	0.999 91	11 920	370	12 290	
4 (GA)	1	48	183	0.95	0.9999	0.952	0.999 91	11 920	500	12 420	1.1%
5 (IM)	1	24	91	0.95	0.9999	0.952	1.000 00	11 920	0	11 920	
5 (GA)	1	24	91	0.95	0.9999	0.952	1.000 00	11 920	180	12 100	1.5%
6 (IM)	1	24	365	0.95	0.9999	0.952	0.999 90	11 920	1820	13 740	
6 (GA)	1	24	365	0.95	0.9999	0.952	0.999 91	11 920	1900	13 820	0.6%

Table 7. Comparison of redundancy and spares allocation for Phase 1.

Case	Algorithm	y_1	y_2	y_3	s_{11}	s_{12}	s_{13}	s_{21}	s_{22}	s_{23}	s_{24}	s_{25}	s_{31}	s_{32}	s_{33}	s_{34}	Total spares	Time (s)
1	IM	5	7	6	0	0	0	1	1	0	0	0	0	0	0	0	2	3012
	GA	5	7	6	0	0	0	1	1	0	0	0	1	0	0	0	3	<20
2	IM	3	6	5	1	1	0	1	1	1	1	0	0	0	0	0	6	3114
	GA	3	6	5	1	1	0	1	1	1	1	0	0	0	0	0	6	<20
3	IM	3	4	3	1	1	0	1	1	1	1	1	1	1	1	1	11	3002
	GA	3	4	3	2	1	0	1	1	1	1	1	1	1	1	1	12	<20
4	IM	5	7	6	0	0	0	1	1	0	0	0	0	0	0	0	2	3185
	GA	5	7	6	0	0	0	1	1	0	0	0	0	1	0	0	3	<20
5	IM	5	7	6	0	0	0	0	0	0	0	0	0	0	0	0	0	3141
	GA	5	7	6	0	0	0	1	0	0	0	0	0	0	0	0	1	<20
6	IM	5	7	6	0	0	0	2	2	2	1	1	1	1	0	0	10	3268
	GA	5	7	6	1	0	0	2	2	2	1	1	1	1	0	0	11	<20

1 to 0.5 year. Use the example of GA, the total mass drops to 8440 kg due to reduced redundancy. However, the spare parts mass is increased to 1830 kg as opposed to 490 kg in Case 1. This case shows that sparing is preferred for a short endurance mission.

Cases 4 investigate how hands-on replacement time influences redundancy and sparing. We let t_{HR} increase from 24 to 48 h. In comparison with Case 1, the mass remains unchanged for IM, and there is 10 kg increase for GA. It shows a reasonable extension of t_{HR} has limited impact on the system design.

Cases 5 and 6 examine how the inventory resupply lead time influences the redundancy and sparing policy. If t_{LT} is reduced from 183 to 91 d, IM shows the sparing is unnecessary, and for GA only one spare unit is needed. However, if t_{LT} doubles and reaches 365 d, 10 or 11 spare parts are required to achieve the 0.9999 availability, as opposed to 2 or 3 in Case 1. Both cases show that t_{LT} plays a critical role in spare parts provisioning. The redundancy of Cases 5 and 6 is identical to Case 1.

6.3. Results and discussion of Phase 2 model

Based on the results of Phase 1 design, we solve Model SSTP in Phase 2 to determine the propellant type, fuel mass, and the spacecraft trajectory to minimize the total launch mass including the payload. The spacecraft is designed with three separable rocket stages. Each stage offers one burn and provides the thrust needed to achieve the velocity change between two nodes. After the burn, the current stage is abandoned to lower the structural mass for the next flight. A three-stage, three-burn rocket requires two transfer nodes to reach LSP after burning all the stages.

Table 8 summarizes the optimization results of rocket staging and spacecraft trajectory for Cases 1–6. The payload mass is the ECLSS and the spare parts from Phase 1 model. In all cases, trajectory (1, 2, 7, 9) is chosen as the optimal route, namely departing from EES to LEO, and further to LLO before descending on LSP. Case 1 is presented for both IM and GA results. It shows the total launch mass is 1555.4 tons for 12.29 tons of payload in IM. The launch mass increases to

Table 8. Optimal rocket staging and trajectory for Phase 2 model (mass unit: ton).

Case	1 (IM)	1 (GA)	2 (GA)	3 (GA)	4 (GA)	5 (GA)	6 (GA)
Payload (ton)	12.29	12.41	10.71	8.44	12.42	12.1	13.82
Trajectory	1-2-7-9	1-2-7-9	1-2-7-9	1-2-7-9	1-2-7-9	1-2-7-9	1-2-7-9
Propellant	LOX-LH2	LOX-LH2	LOX-LH2	LOX-LH2	LOX-LH2	LOX-LH2	LOX-LH2
m_P of Stage 3	8.2	8.2	7.1	5.6	8.2	8.0	9.2
$m_P + m_S$ of Stage 3	9.3	9.4	8.1	6.4	9.4	9.1	10.4
m_P of Stage 2	40.0	40.3	34.8	27.4	40.4	39.3	44.9
$m_P + m_S$ of Stage 2	45.5	46.0	39.7	31.3	46.0	44.8	51.2
m_P of Stage 1	1365.4	1378.7	1189.8	937.7	1379.8	1344.3	1535.4
$m_P + m_S$ of Stage 1	1488.3	1502.8	1296.9	1022.0	1504.0	1465.3	1673.5
Total launch mass	1555.4	1570.6	1355.4	1068.1	1571.8	1531.3	1749.0

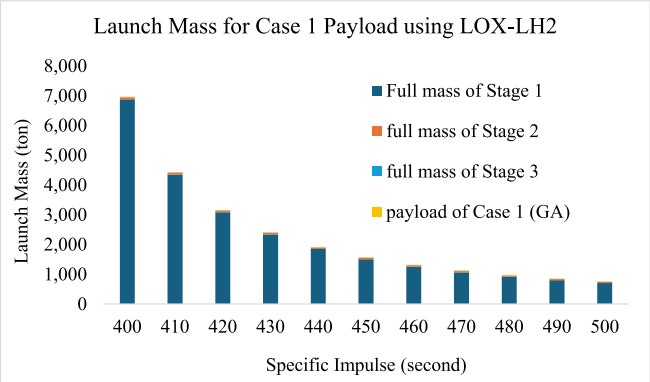

Figure 6. Total launch mass for different I_{sp} using Case 1 PAYLOAD.

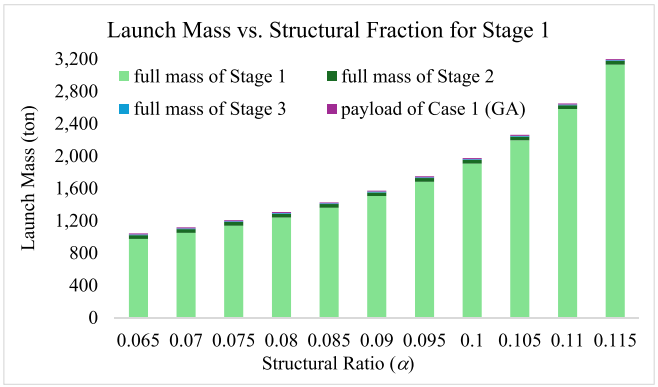

Figure 7. Total launch mass for different α in Stage 1 design.

1570.6 tons for 12.41 tons of payload in GA. Thus, Phase 1 decision plays a critical role in sizing the optimal rocket mass.

The total launch mass of Cases 2–6 is solved based on the payload mass obtained from GA in Phase 1. Similar observations can be made on how the payload mass influences the mass of individual stages and the launch mass. For example, by comparing Cases 1 (GA) and 2 (GA), the launch mass is saved by 215.1 tons, or 14%, when the payload mass is reduced by 1.7 tons.

6.4. Sensitivity analysis

Using Case 1 (GA) payload with 12.41 tons, sensitivity analysis is performed to examine how the Phase 2 model parameters influence the total launch mass. First, Model SSTP is solved, respectively, by increasing I_{sp} from 400 s to 500 s. Figure 6 shows the total launch mass comprised of the payload and three propulsion stages under different I_{sp}. It is found that larger I_{sp} can significantly reduce the launch mass. For example, the total launch mass is 1570.6 tons for $I_{sp} = 450$ s, and it drops to 757.2 tons for $I_{sp} = 500$ s, or 52% mass reduction. However, if I_{sp} is only 400 s, the total launch mass rises to 6964.9 tons, which is 4.4 times that of $I_{sp} = 450$ s.

Next, we examine how structural ratio α influences the total launch mass. In Case 1, $\alpha = 0.09$ is assumed for Stage 1, and $\alpha = 0.14$ for Stages 2 and 3 for LOX-LH2. We let α vary between 0.065 and 0.115 for Stage 1 while keeping $\alpha = 0.14$ for Stages 2 and 3. Model SSTP is solved respectively, and the resulting mass data are shown in figure 7. It is observed that smaller α can effectively reduce the launch mass. For instance, the launch mass is only 1041 tons for $\alpha = 0.065$, which is 33.7% less than that with $\alpha = 0.09$. However, for $\alpha = 0.115$, the total mass increases to 3196 tons or twice the mass with $\alpha = 0.09$.

Finally we examine how the structural ratio of Stages 2 and 3 influences the total launch mass. Assume α varies between 0.09 and 0.19 in Stages 2 and 3 design while keeping $\alpha = 0.09$ for Stage 1. Model SSTP is solved respectively, and the launch masses are shown in figure 8. As expected, smaller α is preferred as it saves the launch mass. For instance, the total mass drops to 1391 tons for $\alpha = 0.09$, or 11.4% lower than that with $\alpha = 0.14$. However, a smaller value of α in Stage 1 can reduce the launch mass more significantly if one compares figure 7 with 8.

6.5. Model assumption and limitation

Our model assumes the ECLSS is a series-parallel configuration. In reality, certain parts may simultaneously provide functions to multiple subsystems. For instance, an air pump could be used for both OG and AR subsystems. We assume components fail independently, but correlated failures are common in complex systems. Both discrete and continuous time Markov chains can be used to model dependent failures. In addition, the spacecraft flight is also assumed to be perfect

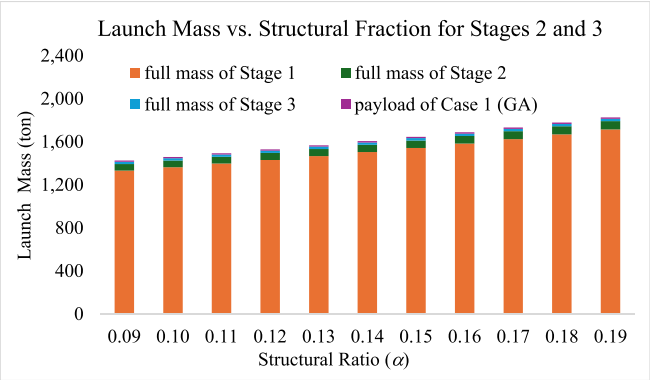

Figure 8. Total launch mass for different α in Stages 2 and 3 design.

with no reliability failure, which may not be always true. In the current model, mass is the primary design metric, but volume and time also play an important role in rocket design, particularly in inter-planetary missions between Earth and Mars.

7. Conclusion

In this paper a redundancy-sparing-trajectory model is proposed to deploy and sustain the long-term human presentence on the Moon in a complex and costly logistics setting. The goal is to minimize the total launch mass of the spacecraft, including LH and spare parts, while achieving the reliability and availability goal. Meta-heuristic and Dijkstra's algorithms are used to search for the optimal solutions. The study represents an early attempt to integrate space logistics into RR and spares inventory allocation, which lays the foundation for future manned mission reliability design in deep space exploration. Numerical experiments show there exists strong interdependency of reliability, redundancy, system availability, sparing policy, resupply lead-time, propellant type, rocket staging, and vehicle trajectory. Redundancy is preferred for short-term mission while sparing is more cost effective for long endurance habitation. A habitation facility requiring extremely high availability is not equivalent to a system having extremely high reliability. Redundancy and spares decisions are closely correlated with reliability and mission duration, but sparing is also highly dependent on the re-supply frequency.

Future study can extend the current work in several directions. For instance, we can assume the spacecraft is reusable and can return to Earth after delivering the cargo and crew to the Moon base. This would significantly reduce the cis-lunar transportation cost. We can also leverage on-demand manufacturing technologies such as 3D printing to produce spare parts for habitation system maintenance. Last but not least, by deploying ISRU systems, lunar regolith can be extracted to produce oxygen, water, fuels and other essential materials, thus achieving self-sustainment on the Moon and beyond.

Appendix. Lower and Upper Limits of Redundancy and Module Availability

I. Estimating the lower limit of y_u based on the ${R_{\mathrm{LH}}}^{\min}$.
Let ${y_u}^{\mathrm{LL}}$ be the lower limit of y_u. For any subsystem for $u = 1, 2, \ldots, U$, its reliability must satisfy the following condition

$$1-\left(1-\prod_{v=1}^{V_u}\mathrm{e}^{-\lambda_{uv}t}\right)^{y_u^{LL}} \geqslant R_{\mathrm{LH}}^{\min}. \tag{A1}$$

Solving equation (A1) yields,

$$y_u^{\mathrm{LL}} \leqslant \frac{\ln\left(1-R_{\mathrm{LH}}^{\min}\right)}{\ln\left(1-\prod_{v=1}^{V_u}\mathrm{e}^{-\lambda_{uv}t}\right)}, \text{for}\, u=1,2,\ldots,U. \tag{A2}$$

II. Let ${y_u}^{\mathrm{UL}}$ be the upper limit of y_u. Then in theory ${y_u}^{\mathrm{UL}}$ can be obtained by

$$1-\left(1-\prod_{v=1}^{V_u}\mathrm{e}^{-\lambda_{uv}t}\right)^{y_u^{\mathrm{UL}}} = 1. \tag{A3}$$

Unfortunately this results in ${y_u}^{\mathrm{UL}} = \infty$. However, we can obtain the most likely value for y_u, denoted as ${y_u}^{\mathrm{like}}$ as follows

$$1-\left(1-\prod_{v=1}^{V_u}\mathrm{e}^{-\lambda_{uv}t}\right)^{y_u^{\mathrm{like}}} = \left(R_{\mathrm{LH}}^{\min}\right)^{\frac{1}{U}}, \text{for}\, u=1,2,\ldots,U. \tag{A4}$$

Then

$$y_u^{\mathrm{like}} = \frac{\ln\left(1-\left(R_{\mathrm{LH}}^{\min}\right)^{\frac{1}{U}}\right)}{\ln\left(1-\prod_{v=1}^{V_u}\mathrm{e}^{-\lambda_{uv}t}\right)}, \text{for}\, u=1,2,\ldots,U. \tag{A5}$$

Obviously ${y_u}^{\mathrm{like}} > {y_u}^{\mathrm{LL}}$, and ${y_u}^{\max} \cong w \times {y_u}^{\mathrm{like}}$ where w is a weight factor for $w > 1$.

III. From equation (7), the upper limit of the module availability in Subsystem u, denoted as ${A_{m,u}}^{\mathrm{UL}}$, is given as follows

$$A_{m,u}^{\mathrm{UL}} = \prod_{v=1}^{V_u}\left(\frac{\frac{1}{\lambda_{uv}}}{\frac{1}{\lambda_{uv}}+t_{\mathrm{HR}}}\right), \text{for}\, u=1,2,\ldots,U. \tag{A6}$$

The above result is obtained assuming that a spare unit is always available upon failure, hence the downtime is t_{HR} only. On the other hand, if no spare part is available upon failure, the lower limit of the module availability, denoted as ${A_{m,u}}^{\mathrm{LL}}$, is obtained as follows

$$A_{m,u}^{\mathrm{LL}} = \prod_{v=1}^{V_u}\left(\frac{\frac{1}{\lambda_{uv}}}{\frac{1}{\lambda_{uv}}+t_{\mathrm{HR}}+t_{\mathrm{LT}}}\right), \text{for}\, u=1,2,\ldots,U. \tag{A7}$$

The worst downtime duration of the module is $t_{\mathrm{HR}} + t_{\mathrm{LT}}$ due to the stockout condition.

References

Ardakan M A, Sima M, Zeinal Hamadani A and Coit D W 2016 A novel strategy for redundant components in reliability–redundancy allocation problems *IIE Trans.* **48** 1043–57

Baraniecka A 2019 Space logistics: current status and perspectives *Trans. Econ. Logist.* **82** 67–78

Blossey G 2023 A stochastic modeling approach for interplanetary supply chain planning *Space Sci. Technol.* **3** 1–14

Chen Z, Zhang H, Wang X, Yang J and Dui H 2024 Reliability analysis and redundancy design of satellite communication system based on a novel Bayesian environmental importance *Reliab. Eng. Syst. Saf.* **243** 109813

Coit D W and Zio E 2019 The evolution of system reliability optimization *Reliab. Eng. Syst. Saf.* **192** 106259

Detrell G, Messerschmid E and Ponsati E G 2016 ECLSS reliability analysis tool for long duration spaceflight *Proc. 46th Int. Conf. on Environmental Systems* (*Vienna, Austria*, *10–14 July*) p 11

Fink W, Baker V R B, Brooks A J-W, Flammia M, Dohm J M and Tarbell M A 2019 Globally optimal rover traverse planning in 3D using Dijkstra's algorithm for multi-objective deployment scenarios *Planet. Space Sci.* **179** 104707

Franciosi C, Lambiase A and Miranda S 2017 Sustainable maintenance: a periodic preventive maintenance model with sustainable spare parts management *IFAC Paper OnLine* **50** 13692–7

Galluzzi M, Zapata E, Steele M and de Weck O 2006 Foundations of supply chain management for space application *Space 2006 Conf. Proc. (AIAA 2006–7234)* (American Institute of Aeronautics and Astronautics) pp 1–17

Goodliff K, Stromgren C, Ewert M, Hill J and Moore C 2017 Logistics needs for future human exploration beyond low Earth orbit *AIAA SPACE and Astronautics Forum and Exposition* (https://doi.org/10.2514/6.2017-5122)

Ho K, de Weck O L, Hoffman J A and Shishko R 2014 Dynamic modeling and optimization for space logistics using time-expanded networks *Acta Astronaut.* **105** 428–43

Ishimatsu T, de Weck O L, Hoffman J A, Ohkami Y and Shishko R 2016 Generalized multicommodity network flow model for the Earth–Moon–Mars logistics system *J. Spacecr. Rockets* **53** 25–38

Jaarsveld W and Dekker R 2011 Spare parts stock control for redundant systems using reliability centered maintenance data *Reliab. Eng. Syst. Saf.* **96** 1576–86

Jiang H, Rodríguez L F and Capristan F 2011 Prediction of reliability for environmental control and life support systems *J. Spacecr. Rockets* **48** 336–45

Jin T, Si S and Zhu W 2024 Allocating redundancy, maintenance and spare parts for minimizing system cost under decentralized repairs *Front. Eng. Manage.* **11** 377–95

Jin T, Taboada H, Espiritu J and Liao H 2017 Allocation of reliability–redundancy and spares inventory under Poisson fleet expansion *IISE Trans.* **49** 737–51

Jones H W 2018 The recent large reduction in space launch cost *Proc. Int. Conf. on Environmental Systems* (*Albuquerque, NM*) pp 1–10 (available at: https://ntrs.nasa.gov/citations/20200001093)

Jones H W 2019 High reliability requires more than providing spares *Proc. 41st Int. Conf. on Environmental Systems* (*Boston, MA, USA, 11–14 July 2010*) p 12

Karabağ O, Eruguz A S and Basten R 2020 Integrated optimization of maintenance interventions and spare part selection for a partially observable multi-component system *Reliab. Eng. Syst. Saf.* **200** 106955

Kim H and Kim P 2017 Reliability–redundancy allocation problem considering optimal redundancy strategy using parallel genetic algorithm *Reliab. Eng. Syst. Saf.* **159** 153–60

Klem M D 2017 LOX/Methane in-space propulsion systems technology status and gaps *Southwest Emerging Technology Symp. (SETS) 2017* (available at: https://ntrs.nasa.gov/api/citations/20170005557/downloads/20170005557.pdf) (Accessed 15 November 2024)

Li X-Y, Liu X, Feng J, Li C, Xiong X and Huang H-Z 2023 Reliability analysis and optimization of multi-phased spaceflight with backup missions and mixed redundancy strategy *Reliab. Eng. Syst. Saf.* **237** 109373

Lin K-P, Luo Y-Z and Tang G-J 2014 Optimization of logistics strategies for long-duration space-station operation *J. Spacecr. Rockets* **51** 1709–20

Nelson S 2024 Moon race 2.0: why so many nations and private companies are aiming for lunar landings (BBC) (available at: www.bbc.com/future/article) (Accessed 20 January 2025)

Olde Keizer M C A, Teunter R H and Veldman J 2017 Joint condition-based maintenance and inventory optimization for systems with multiple components *Eur. J. Oper. Res.* **257** 209–22

Ouyang Z, Liu Y, Ruan S-J and Jiang T 2019 An improved particle swarm optimization algorithm for reliability-redundancy allocation problem with mixed redundancy strategy and heterogeneous components *Reliab. Eng. Syst. Saf.* **181** 62–74

Owens A and de Weck O L 2018 International Space Station operational experience and its impacts on future mission supportability *Proc. 41st Int. Conf. on Environmental Systems* (*Albuquerque, New Mexico, USA*, 8–12 July 2018) p 18

Peiravi A, Nourelfath M and Zanjani M K 2022 Redundancy strategies assessment and optimization of k-out-of-n systems based on Markov chains and genetic algorithms *Reliab. Eng. Syst. Saf.* **221** 108277

Romero E and Francisco D 2020 The NASA human system risk mitigation process for space exploration *Acta Astronaut.* **175** 606–15

Sawik B 2023 Space mission risk, sustainability and supply chain: review, multi-objective optimization model and practical approach *Sustainability* **15** 11002

Si S, Liu M, Jiang Z, Jin T and Cai Z 2019 System reliability allocation and optimization based on generalized Birnbaum importance measure *IEEE Trans. Reliab.* **68** 831–43

Sleptchenko A and van der Heijden M 2016 Joint optimization of redundancy level and spare part inventories *Reliab. Eng. Syst. Saf.* **153** 64–74

Taylor C and de Weck O L 2005 Concurrent trajectory and vehicle optimization: a case study of Earth-Moon supply chain logistics *Proc. 46th AIAA/ASME/ASCE/AHS/ASC Structures, Structural Dynamics & Materials Conf.* p 13

Taylor C, Song M, Klabjan D, de Weck O and Simchi-Levi D 2007 A mathematical model for interplanetary logistics *Logist. Spectr.* **41** 23–33 (available at: www.semanticscholar.org/paper/A-mathematical-model-for-interplanetary-logistics-Taylor/c1c1dcbe41ab5a398a58607b4e3010b570656dc8?utm_source=direct_link)

Wang W 2012 A stochastic model for joint spare parts inventory and planned maintenance optimisation *Eur. J. Oper. Res.* **216** 127–39

Wang W and Syntetos A A 2011 Spare parts demand: linking forecasting to equipment maintenance *Trans. Res.* E **47** 1194–209

West W, Samplatsky D and Locks W 2016 Lunar surface habitats as a development opportunity for Mars surface life support systems *Proc. 46th Int. Conf. on Environmental Systems*

(ICES-2016-226) (*Vienna, Austria*) p 12 (available at: http://hdl.handle.net/2346/67609)
Wu X and Wu X 2017 An importance-based algorithm for reliability redundancy allocation of phased mission systems *Proc. 2017 IEEE Int. Conf. on Software Quality, Reliability and Security* (*Prague, Czech Republic*) pp 152–9
Xie W, Liao H and Jin T 2014 Maximizing system availability through joint decision on component redundancy and spares inventory *Eur. J. Oper. Res.* **237** 164–76
Yan T, Lei Y, Wang B, Han T, Si X and Li N 2020 Joint maintenance and spare parts inventory optimization for multi-unit systems considering imperfect maintenance actions *Reliab. Eng. Syst. Saf.* **202** 106994
Zaretalab A, Hajipour V and Tavana M 2020 Redundancy allocation problem with multi-state component systems and reliable supplier *Reliab. Eng. Syst. Saf.* **193** 106629
Zhang H, Tian Z and Zuo M 2024 Component-level wind farm maintenance considering seasonal uncertainties *Proc. 2024 IEEE Int. Conf. on Prognostics and Health Management (ICPHM)* (*Spokane, WA, USA*) (https://doi.org/10.1109/ICPHM61352.2024.10626855)
Zhao X, Zhang J and Wang X 2018 Joint optimization of components redundancy, spares inventory and repairmen allocation for a standby series system *Proc. Inst. Mech. Eng.* O **233** 1–16
Zheng M, Ye H, Wang D and Pan E 2021 Joint optimization of condition-based maintenance and spare parts orders for multi-unit systems with dual sourcing *Reliab. Eng. Syst. Saf.* **210** 107512
Zhu S, van Jaarsveld W and Dekker R 2020 Spare parts inventory control based on maintenance planning *Reliab. Eng. Syst. Saf.* **193** 106600
Zhu X, Wang J and Coit D W 2024 Joint optimization of spare part supply and opportunistic condition-based maintenance for onshore wind farms considering maintenance route *IEEE Trans. Eng. Manage.* **71** 1086–102

Tongdan Jin Dr Tongdan Jin is a professor in the Ingram School of Engineering at Texas State University. He received the Ph.D. in industrial and systems engineering from Rutgers University-New Brunswick, USA. Prior to academia, he had 5 year industry experience in reliability design and after-sales support of semiconductor equipment in Teradyne Inc., Boston. Dr Jin has authored and co-authored a broad range of publications in system reliability optimization, transportation electrification, renewable energy, and net-zero supply chain operations. The works are shown in IEEE Transactions on Reliability, IEEE Transactions on Smart Grid, IISE Transactions, and European Journal of Operational Research. He authored a book entitled "Reliability Engineering and Services" published by Wiley in 2019. He garnered several best paper awards, including the Evans-McElroy best paper in Reliability and Maintainability Symposium. He has served as a reviewer and panelist in NSF CAREER proposals since 2018. He served as the associate editor of IISE Transactions from 2017 to 2021, and currently serves as a steering committee member of IEEE Intelligent Systems to Human-Aware Sustainability, and editorial board of Journal of Reliability Science and Engineering. He is affiliated with societies of IEEE, INFORMS and IISE.

Ahsanul Abedin Ahsanul Abedin is pursuing his Master's in Industrial Engineering and serves as a Graduate Instructional Assistant in the Ingram School of Engineering at Texas State University. He holds a Bachelor's degree in Industrial and Production Engineering from Khulna University of Engineering and Technology, Bangladesh, where his thesis focused on Total Productive Maintenance. After graduation, he collaborated on research into Integrated Management Systems. His current interests lie in Reliability Engineering, Maintenance, and Spare Parts Logistics, with a vision to apply these concepts to extraterrestrial environments such as the Moon and Mars.